Journal of Geophysical Research-Oceans

Supporting Information for

Characterization of Bio-optical Anomalies in the Kerguelen Region, Southern Indian Ocean: A study Based on Shipborne Sampling and BioGeoChemical-Argo Profiling Floats

J. Uitz[1], C. Roesler[2], E. Organelli[3], H. Claustre[1], C. Penkerc'h[1], S. Drapeau[2], E. Leymarie[1], A. Poteau[1], C. Schmechtig[4], C. Dimier[5], J. Ras[1], X. Xing[6], S. Blain[7]

[1]CNRS and Sorbonne Université, Laboratoire d'Océanographie de Villefranche (LOV), UMR 7093, 06230 Villefranche-sur-Mer, France.

[2]Bowdoin College, Earth and Oceanographic Science, Brunswick, Maine 04011, USA.

[3]National Research Council (CNR), Institute of Marine Sciences (ISMAR), 00133 Rome, Italy.

[4]CNRS and Sorbonne Université, OSU Ecce Terra, UMS 3455, 75252 Paris Cedex 05, France.

[5]CNRS and Sorbonne Université, Institut de la Mer de Villefranche (IMEV), FR 3761, 06230 Villefranche-sur-Mer, France.

[6]State Key Laboratory of Satellite Ocean Environment Dynamics (SOED), Second Institute of Oceanography, Ministry of Natural Resources, Hangzhou, China.

[7]CNRS and Sorbonne Université, Laboratoire d'Océanographie Microbienne (LOMIC), UMR 7621, Banyuls-sur-Mer, France.

Contents of this file

Introduction

This supporting information file contains five figures. Figure S1 shows the spectra of the chlorophyll-specific phytoplankton absorption coefficient for each of the SOCLIM cruise sampling stations and each sampling depth. Figure S2 presents scatterplots of the Fuco, Peri, Hex, TChlb, Zea, and Pras ratios to TChla and their relationships with the phytoplankton blue-to-red absorption ratio and TChla values. Figure S3 shows the spectra of the absorption coefficient by colored dissolved organic matter for 9 of the SOCLIM cruise sampling stations and for each sampling depth. Figure S4 shows ternary plots of the relative contributions to absorption of phytoplankton, non-algal particles and color dissolved organic matter at two wavelengths, 380 and 490 nm, for 9 of the SOCLIM cruise sampling stations. Finally, Figure S5 displays the mean annual cycle of the $K_{bio}(380)$ coefficient derived from the BGC-Argo float observations for the 5 regions of the SO considered in the study.

This supporting information file also includes Text S1, which presents our approach for estimating the diffuse attenuation coefficient, $\widehat{\mathrm{K}}_{\mathrm{d}}$, based on Monte Carlo modeling, for the purpose of comparison with the $K_{bio}(490)$ coefficient derived from the BGC-Argo float measurements.

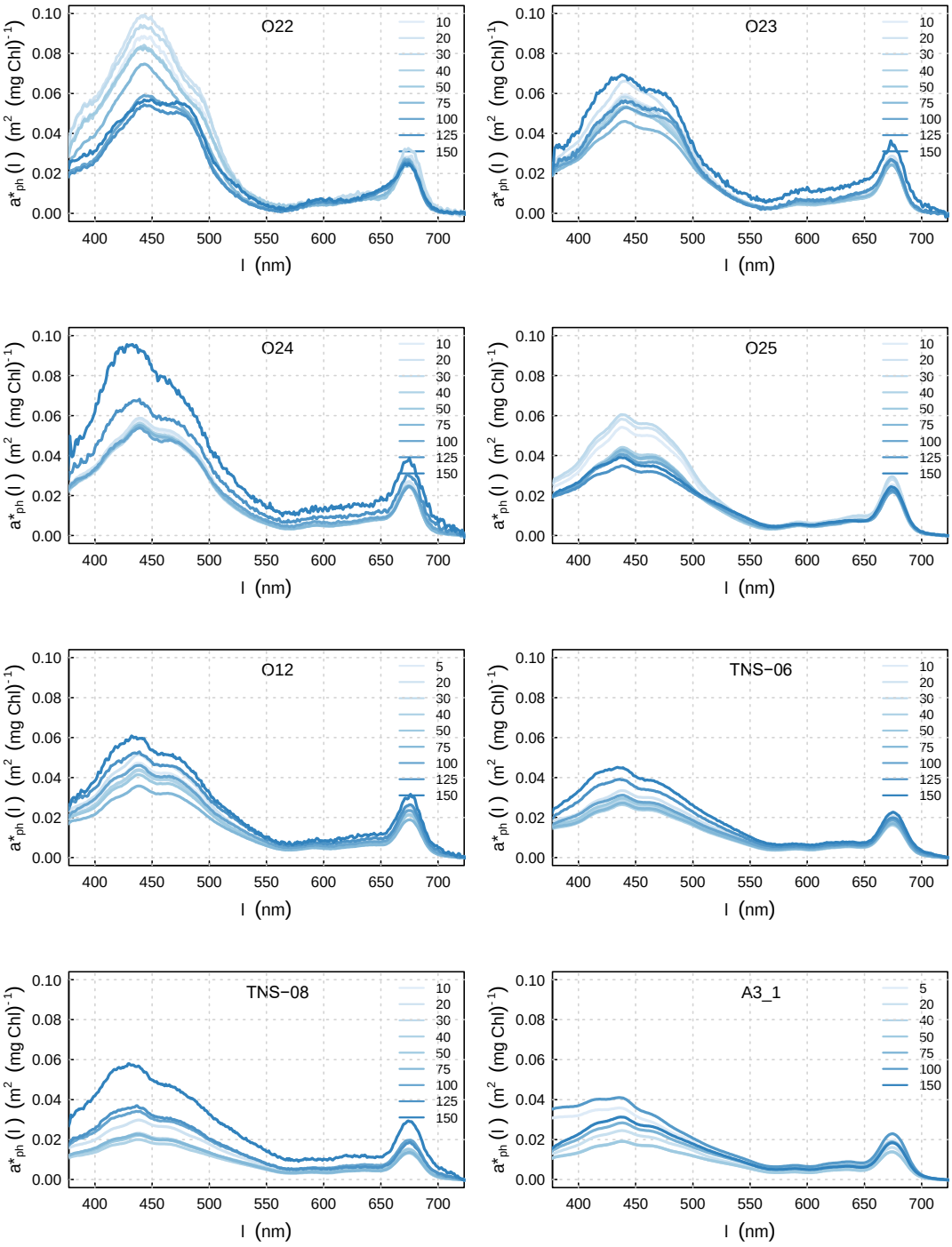

Figure S1. Spectra of the chlorophyll-specific phytoplankton absorption coefficient, $a_{ph}(\lambda)$, for each station of the SOCLIM cruise. The different colors of the curves correspond to the sampling depth (in m) as indicated on each panel.

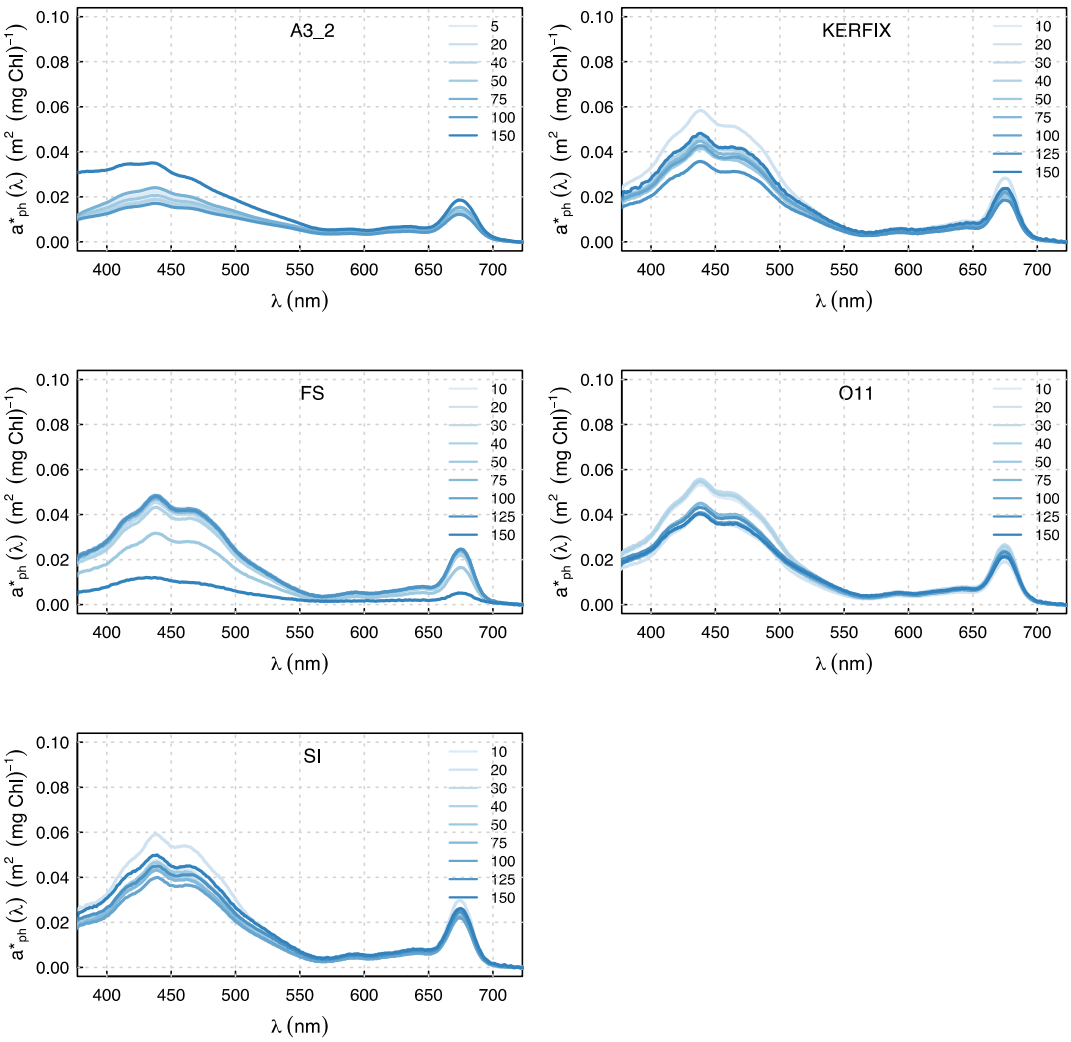

Figure S1 (continued). Spectra of the chlorophyll-specific phytoplankton absorption coefficient, $a_{ph}(\lambda)$, for each station of the SOCLIM cruise. The different colors of the curves correspond to the sampling depth (in m) as indicated on each panel.

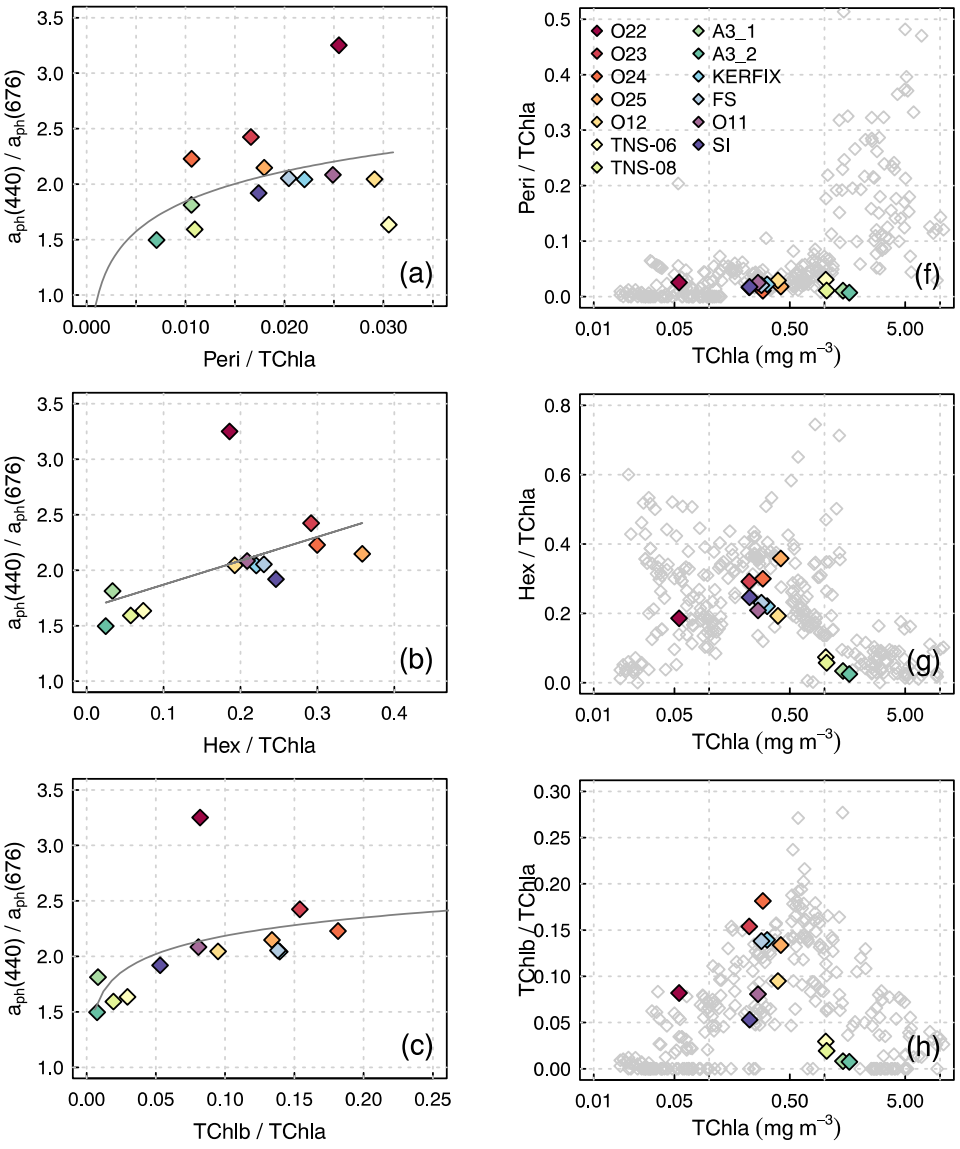

Figure S2. Scatterplots of the distribution of (left column) the $a_{ph}(440) / a_{ph}(676)$ ratio as a function of the ratios to TChla of selected pigments, and (right column) the ratios to TChla of selected pigments a function of TChla. Specifically, the selected pigments are (a and f) Peri; (b and g) Hex; and (c and h) TChlb. Only surface data are shown. The color key indicates the SOCLIM cruise sampling stations. Lines indicate best linear or lognormal fits. When available, we show in grey color previously published measurements from the Subequatorial Pacific Ocean, Atlantic Ocean and Mediterranean Sea (Bricaud et al., 2004) and from the Southeast Pacific Ocean (Bricaud et al., 2010).

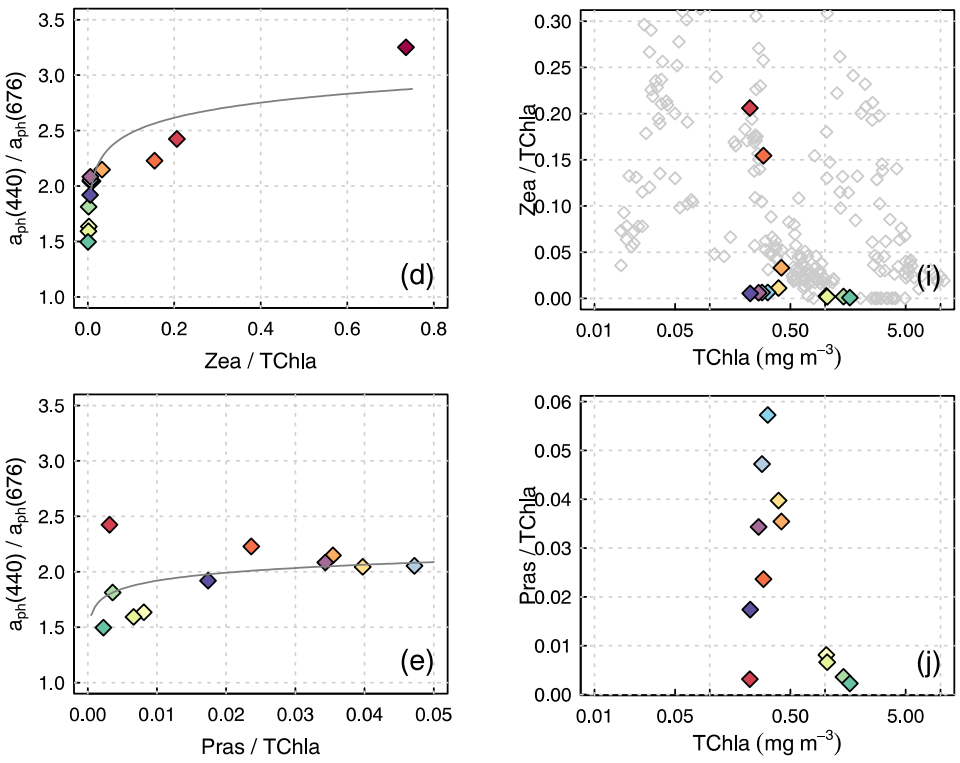

Figure S2 (continued). Scatterplots of the distribution of (left column) the $a_{ph}(440)$ / $a_{ph}(676)$ ratio as a function of the ratios to TChla of selected pigments, and (right column) the ratios to TChla of selected pigments a function of TChla. Specifically, the selected pigments are (d and i) Zea; and (d and i) Pras. Only surface data are shown. The color key indicates the SOCLIM cruise sampling stations. Lines indicate best linear or lognormal fits. When available, we show in grey color previously published measurements from the Subequatorial Pacific Ocean, Atlantic Ocean and Mediterranean Sea (Bricaud et al., 2004) and from the Southeast Pacific Ocean (Bricaud et al., 2010).

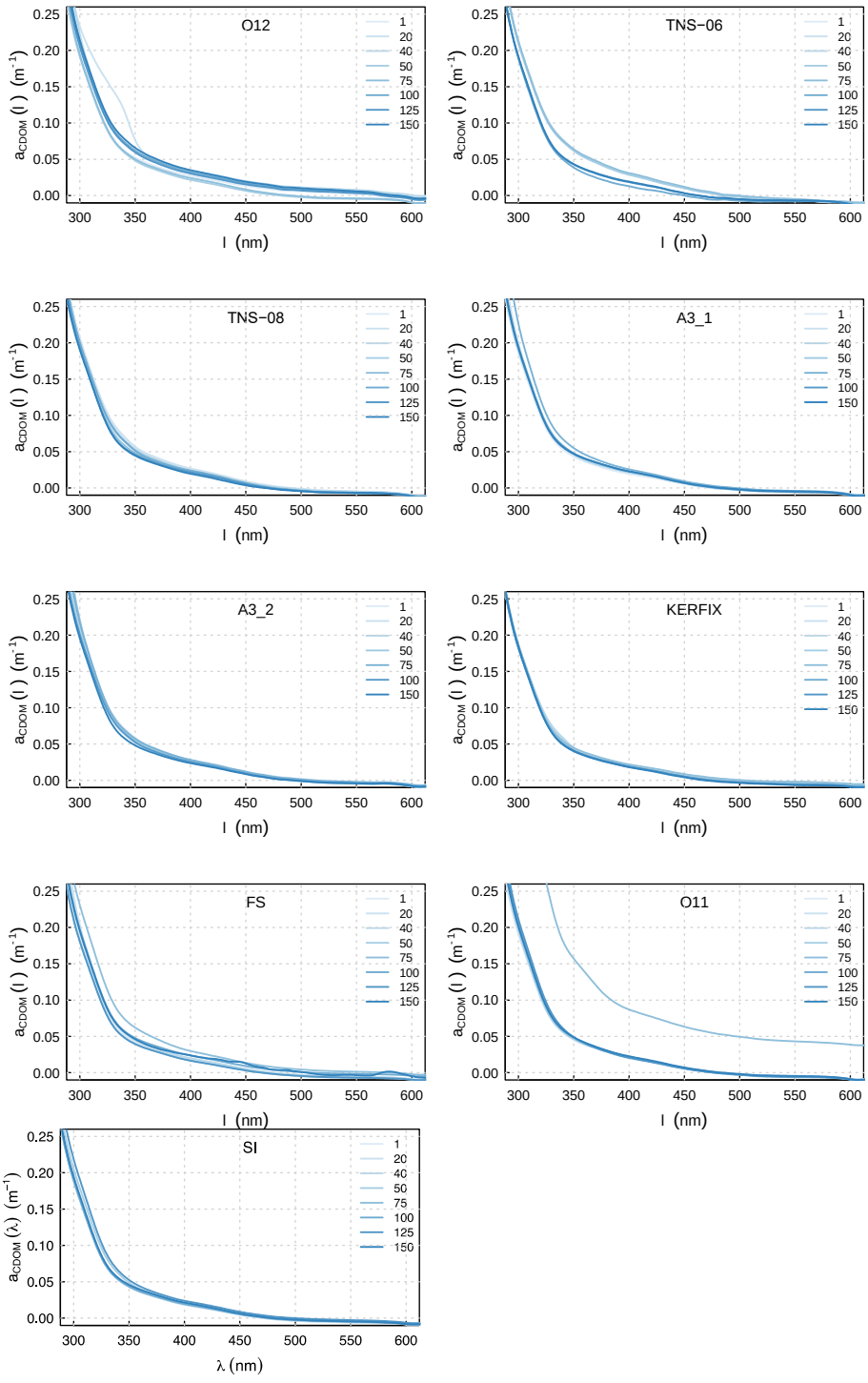

Figure S3. Spectra of the colored dissolved organic matter absorption coefficient, $a_{CDOM}(\lambda)$, for 9 stations of the SOCLIM cruise. The different colors of the curves correspond to the sampling depth (in m) as indicated on each panel.

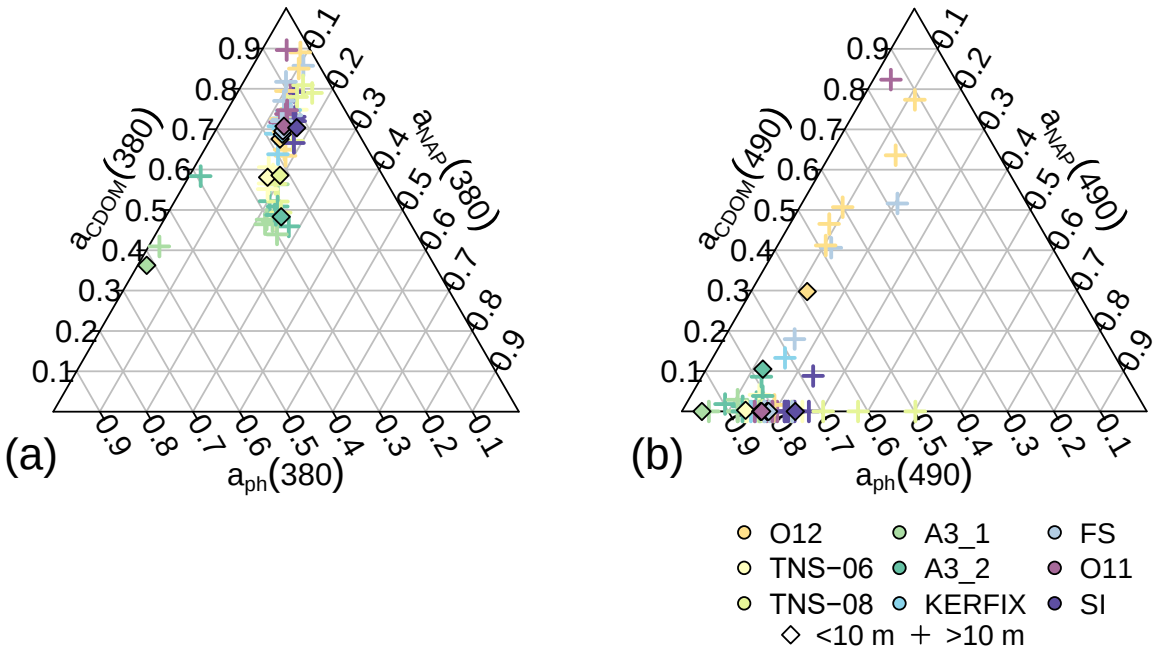

Figure S4. Ternary diagram showing the relative contribution to the absorption coefficient of phytoplankton, $a_{ph}(\lambda)$, non-algal particles, $a_{NAP}(\lambda)$, and colored dissolved organic matter, $a_{CDOM}(\lambda)$ at a wavelength, λ, of (a) 380 nm and (b) 490 nm. The color code indicates the SOCLIM cruise sampling stations and the symbols the depth of acquisition. Values within the layer 0–150 m are shown, with surface data represented by the diamond symbols. The a_{NAP} estimates for station A3 are shown for information purposes but are not considered in the analysis (see Sect. 2.2.3).

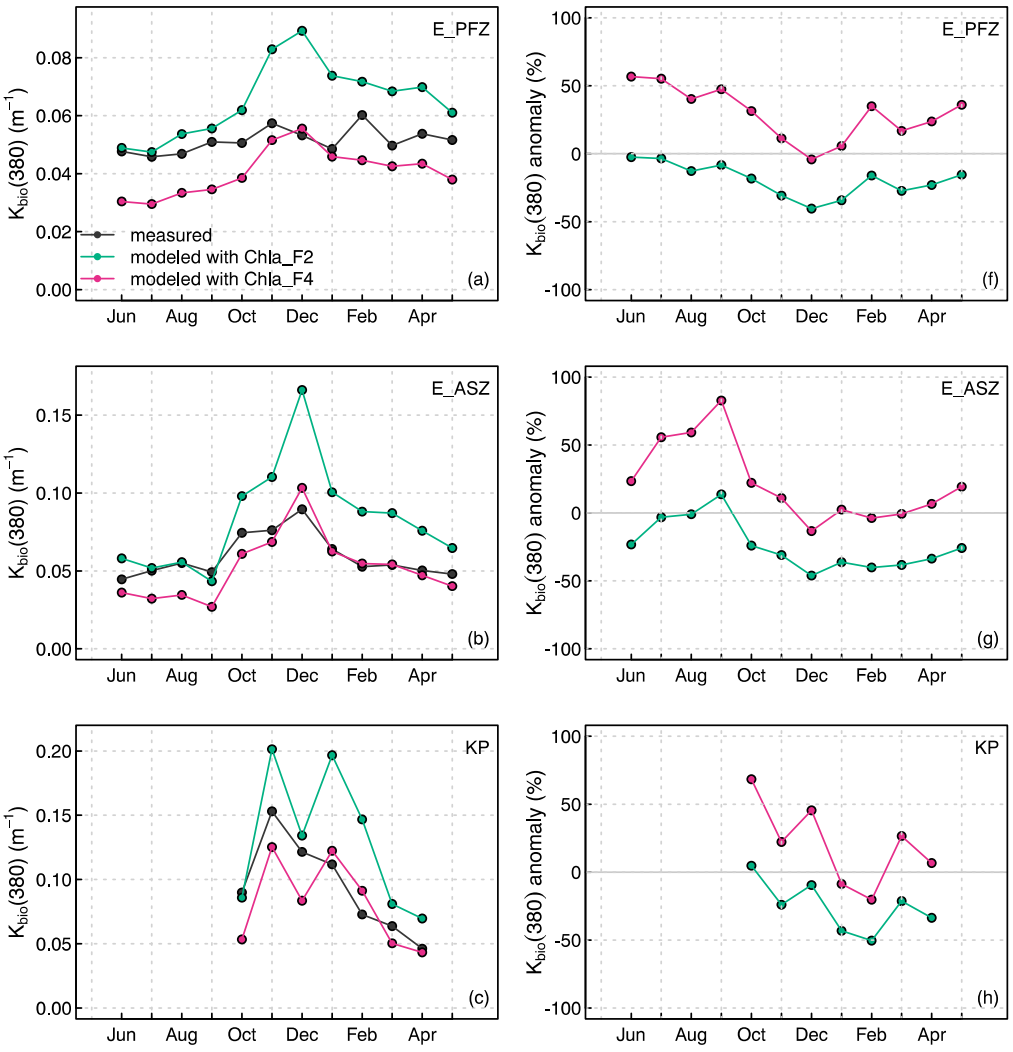

Figure S5. Monthly mean values of (a–c) the diffuse attenuation coefficient for downward irradiance at 380 nm, $K_{bio}(380)$ and (f–h) corresponding anomaly index for (a and f) the East Polar Front Zone, E_PFZ; (b and g) the East Antarctic Southern Zone, E_ASZ; and (c and h) the Kerguelen Plateau, KP. For panels (a–c) the black curve represents the $K_{bio}(380)$ values retrieved from the radiometric measurements of the BGC-Argo floats, the green and pink curves show the $K_{bio}(380)$ values predicted from the general model of Morel & Maritorena (2001), using as input the monthly mean values of BGC-Argo-measured chlorophyll *a* concentration corrected with either a factor of 2 (Chla_F2) or a factor of 4 (Chla_F4), respectively. For panels (f–h), the anomaly index (in %) is calculated as the difference between the monthly mean of the measured $K_{bio}(380)$ values and the predictions from the model of Morel & Maritorena (2001), using as input either the monthly mean values of Chla_F2 (green curve) or Chla_F4 (pink curve), normalized to the predictions.

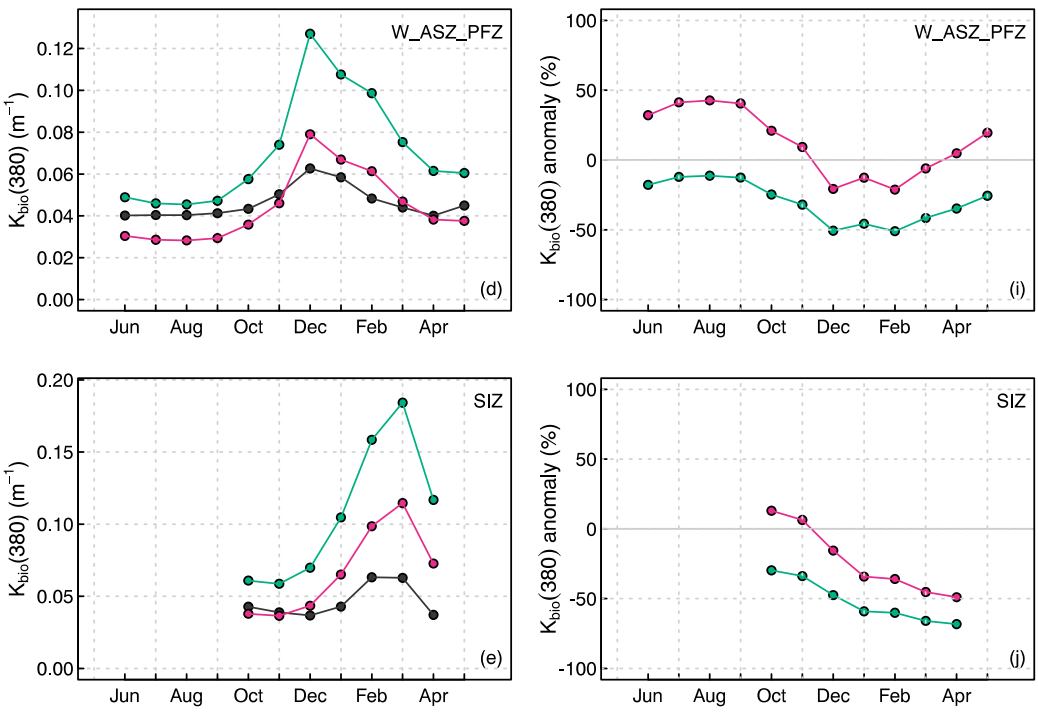

Figure S5 (continued). Monthly mean values of (d–e) the diffuse attenuation coefficient for downward irradiance at 380 nm, $K_{bio}(380)$ and (i–j) corresponding anomaly index for (d and i) the West Polar Front Zone and West Antarctic Southern Zone, W_PFZ_ASZ; and (e and j) the Seasonal Ice Zone, SIZ. For panels (d–e) the black curve represents the $K_{bio}(380)$ values retrieved from the radiometric measurements of the BGC-Argo floats, the green and pink curves show the $K_{bio}(380)$ values predicted from the general model of Morel & Maritorena (2001), using as input the monthly mean values of BGC-Argo-measured chlorophyll *a* concentration corrected with either a factor of 2 (Chla_F2) or a factor of 4 (Chla_F4), respectively. For panels (i–j), the anomaly index (in %) is calculated as the difference between the monthly mean of the measured $K_{bio}(380)$ values and the predictions from the model of Morel & Maritorena (2001), using as input either the monthly mean values of Chla_F2 (green curve) or Chla_F4 (pink curve), normalized to the predictions.

Text S1

For comparison with the $K_{bio}(490)$ coefficient derived from the BGC-Argo float radiometric measurements, we used optical properties measured from the surface flow-through system of the vessel and estimated the diffuse attenuation coefficient, $\widehat{\mathrm{K}}_{\mathrm{d}}$, from Monte Carlo modeling. Below we first present the method used to acquire and process the surface optical measurements and second our approach for estimating the $\widehat{\mathrm{K}}_{\mathrm{d}}$ coefficient.

Absorption, scattering and beam attenuation coefficients

Multispectral absorption, $a(\lambda)$, and beam attenuation, $c(\lambda)$, coefficients were measured on discrete samples collected from the surface flow-through system of the vessel with a WET Labs ac9 instrument. Approximately 2L of samples were run through the a and c tubes of the ac9 in gravity-driven flow-through mode. Samples were subsequently filtered through a Whatman GF/F filter to remove the particulate matter and obtain an estimate of the absorption and beam attenuation coefficients of the filtrate. The selection of this filter size was to ensure closure with the particulate absorption measured spectrophotometrically (Sect. 2.2.3). Absorption and attenuation spectra were corrected for measured sample temperature and salinity (Sullivan et al., 2006) and absorption was corrected for scattering using the proportional method (Zaneveld et al., 1994). The particulate absorption coefficient, $a_p(\lambda)$, was computed from the difference between absorption of the unfiltered and filtered sample. The scattering coefficient, $b(\lambda)$, was computed from the difference between the beam attenuation and absorption coefficients: $b_p(\lambda) = c_p(\lambda) - a_p(\lambda)$.

The particulate backscattering coefficient, $b_{bp}(\lambda)$, at 470 nm, 532 nm and 660, was measured with a WET Labs ECO BB3 in a light-trapping casket (Dall'Olmo et al., 2009) on approximately 4L of seawater sampled from the surface flow-through system. The data were processed in a similar manner as the $b_{bp}(700)$ data acquired in a profile mode from the hydrological CTD casts and BGC-Argo floats (see Sect. 2.2.5), following the standard BGC-Argo protocol given in Schmechtig et al. (2018). Briefly, raw counts from the sensor were converted into the volume scattering function (VSF) at an angle of 124° and a wavelength λ, $\beta(124, \lambda)$, by applying the sensor-specific dark value and a scaling factor provided by the manufacturer. The $b_{bp}(\lambda)$ coefficient was calculated after Boss & Pegau (2001):

$$\mathrm{b_{bp}}(\lambda) = \chi(124)\, 2\pi\, (\beta(124,\lambda) - \beta_{\mathrm{sw}}(124,\lambda)) \qquad \text{(S1)}$$

with $\chi(124)$ the angle-dependent conversion factor equal to 1.076 (Sullivan et al., 2013), and $\beta_{sw}(124,\lambda)$ the salinity- and temperature-dependent contribution of pure water to the VSF computed according to Zhang & Hu (2009).

Modeling of the $\widehat{\mathrm{K}}_{\mathrm{d}}$ coefficient

We estimated the $\widehat{\mathrm{K}}_{\mathrm{d}}$ coefficient following the model of Kirk (1991) derived from Monte Carlo modeling:

$$\widehat{\mathrm{K}}_{\mathrm{d}}(490) = \frac{1}{\mu_{\mathrm{o}}}\sqrt{\mathrm{a}^2 + \mathrm{ab} \times (\mathrm{g}_1 \times \mu_{\mathrm{o}} - \mathrm{g}_2)} \quad \text{(S2)}$$

where μ_o is the average cosine for the refracted solar beam (determined from latitude, date, assuming noontime for clear and overcast skies for each station and the index of refraction for seawater), a and b are the absorption and scattering coefficients at 490 nm obtained from a WETLabs ac9 (see above). The coefficients $\mathrm{g}_1$and g_2 are constants determining the relative contributions of scattering to vertical attenuation of irradiance. Kirk (1991) provides values (see their table 2) from Monte Carlo simulations for 10 water types (see their table 1) defined by the scattering coefficient and the backscattering ratio. This approach was shown to provide robust estimates of measured diffuse attenuation values (Pérez et al., 2016) even for a scenario where independent backscattering coefficients were not measured (Belzile et al., 2002).

Our approach was to calculate the backscattering ratio at 440 nm from:

$$\frac{\mathrm{b}_{\mathrm{b}}(440)}{\mathrm{b}(440)} = \frac{\mathrm{b}_{\mathrm{bp}}(440) + \mathrm{b}_{\mathrm{bw}}(440)}{\mathrm{b}_{\mathrm{p}}(440) + \mathrm{b}_{\mathrm{w}}(440)} \quad \text{(S3)}$$

where the particulate backscattering coefficient at 440 nm was measured with the WET Labs ECO BB3 (see above). It is necessary to add the scattering and backscattering coefficients of pure water to the measured scattering and backscattering coefficients in order to determine accurately the water type and hence the appropriate $\mathrm{g}_1$and g_2 coefficients. The backscattering ratio at 490 nm was then set equal to the backscattering ratio at 440 nm following Ulloa et al. (1994) who demonstrated that while both scattering and backscattering are spectrally dependent, the backscattering ratio does not vary spectrally for oceanic particles. Water types for these stations ranged across 1, 2, and 5 (see Kirk, 1991, table 2). Once the water type and the appropriate g_1 and g_2 coefficients were determined, the diffuse attenuation at 490 nm was computed from Eq. (S2) using the measured absorption and scattering coefficients at 490 nm, *without* adding the optical properties of pure water, so that the modeled $\widehat{\mathrm{K}}_{\mathrm{d}}(490)$ values are analogous to the $K_{bio}(490)$ values calculated from the BGC-Argo float observations which likewise do not include the optical properties of water.